



Correspondence Authors:

Name: Guofeng Zhu^{1,2*}

Institution:

¹ *College of Geography and Environment Science, Northwest Normal University,
Lanzhou 730070, Gansu, China*

² *Shiyang River Ecological Environment Observation Station, Northwest Normal
University, Lanzhou 730070, Gansu, China*

Address:

College of Geography and Environment Science of Northwest Normal
University, 967, East Road, Lanzhou, Gansu, China 730070.

Tel: +86-13909310867

1 **E-mail:** zhugf@nwnu.edu.cn



2 **Global Water Vapor Stable Isotope Dataset**

3 *Dongfei Yang^{a,b,c}, Guofeng Zhu^{a,b,c,d,*}, Jiangwei Yang^{a,b,c}, Rui Li^{a,b,c}, Qinqin Wang^{a,b,c}, Xiaoxiao*

4 *Su^{a,b,c}, Yitian Lei^{a,b,c}, Yurou Zhang^{a,b,c}, Wenjing Liu^{a,b,c}, Kang Ning^{a,b,c}, Xinyue Wang^{a,b,c}, Yaxin Li^{a,b,c}*

5 **Affiliations:**

6 *^a College of Geography and Environment Science, Northwest Normal University, Lanzhou 730070,*

7 *Gansu, China*

8 *^b Shiyang River Ecological Environment Observation Station, Northwest Normal University,*

9 *Lanzhou 730070, Gansu, China*

10 *^c Key Laboratory of Resource Environment and Sustainable Development of Oasis, Gansu*

11 *Province, Lanzhou 730070, Gansu, China*

12 *^d Lanzhou Branch, Remote Sensing Application Center, Ministry of Agriculture and Rural Affairs,*

13 *Lanzhou 730070, Gansu, China*

14

15 **Correspondence to: Guofeng Zhu (zhugf@nwnu.edu.cn)*

16

17 **Abstract:** Stable isotopes in atmospheric water vapor (reported as $\delta^2\text{H}$ and $\delta^{18}\text{O}$

18 relative to VSMOW) provide valuable constraints on moisture sources, transport, and

19 phase-change fractionation. Yet available observations remain fragmented across

20 platforms, regions, and time periods, and cross-study comparison is often hindered by

21 inconsistent metadata, calibration reporting, and quality-control practices. Here we

22 compile and harmonize a global near-surface water vapor isotope dataset from three

23 sources: the WaterIsotopes Database (wiDB; <http://wateriso.utah.edu/waterisotopes>),



24 PANGAEA (<https://www.pangaea.de>), and peer-reviewed literature. The dataset
25 spans 1981–2021 and contains 87,138 records from 112 sites/platforms. We
26 standardized coordinates to WGS84, timestamps to UTC when possible, isotope units
27 to per mil (‰) in delta notation, and compiled measurement metadata (instrument,
28 method, and model where explicitly reported; e.g., Picarro CRDS, LGR OA-ICOS,
29 IRMS following cryogenic trapping, and satellite retrieval products). A transparent
30 quality-control workflow was applied to identify duplicates, inconsistent metadata,
31 and implausible or poorly documented values, while preserving traceability to original
32 sources. The resulting product provides a consistent observational basis for model
33 evaluation and for comparative studies of water vapor isotope variability across
34 climates and observation strategies. The Global Water Vapor Stable Isotope Dataset
35 is available at <https://doi.org/10.6084/m9.figshare.30893984> (Zhu and Yang, 2025).

36 **Keywords:** atmospheric water vapor; stable isotopes; dataset; Spatiotemporal Patterns;
37 quality control

38 **1 Introduction**

39 The water cycle is a central component of the Earth's climate system, and its
40 dynamic variations directly influence the global energy balance, ecosystem succession,
41 and water resource distribution (Shi et al., 2022). Under global change, the water
42 cycle is undergoing significant alterations, with its spatial – temporal distribution and
43 variability showing new characteristics (Ren et al., 2024), such as enhanced
44 evaporation, restructured precipitation patterns, and more frequent extreme
45 hydrological events (Bingham and Bayler, 2025; Colman and Soden, 2021). Stable



46 isotopes, as natural tracers of water vapor transport and phase change processes
47 (Shang et al., 2024), provide a unique perspective for understanding the dynamic
48 mechanisms of the atmospheric water cycle (Gimeno et al., 2020). The fractionation
49 effects of isotopes are closely related to temperature, humidity, vapor source regions,
50 and transport pathways (Xu et al., 2022), making them a link between microscopic
51 phase-change processes and the macroscopic climate system (Galewsky et al., 2016).

52 In recent years, advances in laser absorption spectroscopy have enabled
53 high-frequency and continuous measurements of water vapor isotopes (Wei et al.,
54 2019), while satellite retrievals have made it possible to observe their
55 three-dimensional global distribution (Yang et al., 2023); Multi-platform collaborative
56 observations have preliminarily integrated precipitation, surface water, and water
57 vapor isotope data (Chen et al., 2024; Li et al., 2025); Isotope-enabled general
58 circulation models (iGCMs) (Jouzel et al., 2013; Peng et al., 2020) enhance the
59 analysis of source regions, transport, and phase-change processes by explicitly
60 simulating isotope fractionation (Leroy-Dos Santos et al., 2023). However,
61 inconsistencies in sampling strategies, quality control, and calibration systems among
62 different data sources make cross-regional and intertemporal comparisons susceptible
63 to systematic errors (Voglar et al., 2019).

64 At present, the driving mechanisms underlying variations in water vapor isotopes
65 remain inadequately understood (Galewsky et al., 2023; Xing et al., 2023; Xu et al.,
66 2024). Under global warming, the combined effects of source-region relative humidity,
67 land – sea thermal contrast, convective depth, and re-evaporation cause stable



68 isotopes in water vapor to exhibit pronounced nonlinear responses and spatiotemporal
69 heterogeneity to climatic forcing; Isotopic signals are further modulated by the
70 interplay between multi-scale circulation modes and boundary-layer processes
71 (Saranya et al., 2018), forming complex feedback mechanisms. Without a unified and
72 comparable data framework, it is difficult to robustly disentangle the contributions of
73 source-region conditions, transport pathways, and cloud microphysical processes, or
74 to quantify the marginal role of water vapor recycling in extreme events (Wang et al.,
75 2023a). This theoretical gap constrains the examination of the formation mechanisms
76 and interdecadal variations of the “ first-order spatial framework ” (low-latitude
77 enrichment – high-latitude depletion and progressive depletion from ocean to land).
78 Moreover, recent studies (Gimeno et al., 2021; Lu et al., 2024; Smith and Lacey, 2024;
79 Zhu et al., 2023) show that arid regions exhibit systematic isotope enrichment and
80 rising d-excess, whereas responses in high-latitude and oceanic regions are relatively
81 subdued. Such regionally differentiated responses require integrated analyses based
82 on unified datasets to disentangle multi-process interactions, clarify causal
83 relationships, and identify the critical thresholds and strengths of feedback
84 mechanisms.

85 In arid and semi-arid regions, intensified precipitation variability and
86 evapotranspiration imbalance have exacerbated conflicts between water supply and
87 demand. Isotopic data can be used to identify re-evaporation intensity and the
88 contribution of upstream moisture transport (Fang et al., 2022), providing a scientific
89 basis for drought monitoring and water allocation decisions; In monsoon – westerly



90 interaction zones, phase shifts in moisture pathways and convective activity amplify
91 precipitation extremes. Coupling analyses of d-excess and isotope – climate indicators
92 can identify source-region transitions (Tharammal et al., 2023) and enhanced vapor
93 recycling in advance, which is valuable for early warning of extreme precipitation
94 events; In high-latitude and polar regions, sea-ice melting and the expansion of open
95 water modify local evaporation and boundary-layer structure (Rozmiarek et al., 2025).
96 Abnormal d-excess values provide independent constraints on ice – atmosphere
97 interactions and freshening effects, which are crucial for assessing the hydrological
98 and climatic impacts of sea-ice decline (Klein et al., 2015). The combination of
99 regional challenges and societal demands — such as intensified droughts, greater
100 precipitation variability, and more frequent extreme events — calls for the rapid
101 establishment of standardized datasets and comparable analytical frameworks to
102 support water resource management, extreme event attribution, and climate resilience
103 building (Baijuan et al., 2023).

104 To address the above challenges and demands, this study aims to solve the
105 following core issues: (1) to establish a high-resolution global water vapor isotope
106 dataset; and (2) to identify the dynamic processes of the atmospheric water cycle
107 based on the global water vapor isotope data. The outcomes of this study will provide
108 essential validation benchmarks for global hydroclimate models and support
109 sustainable water resource management and the development of climate-resilient
110 societies.

111 **2 Data and methods**



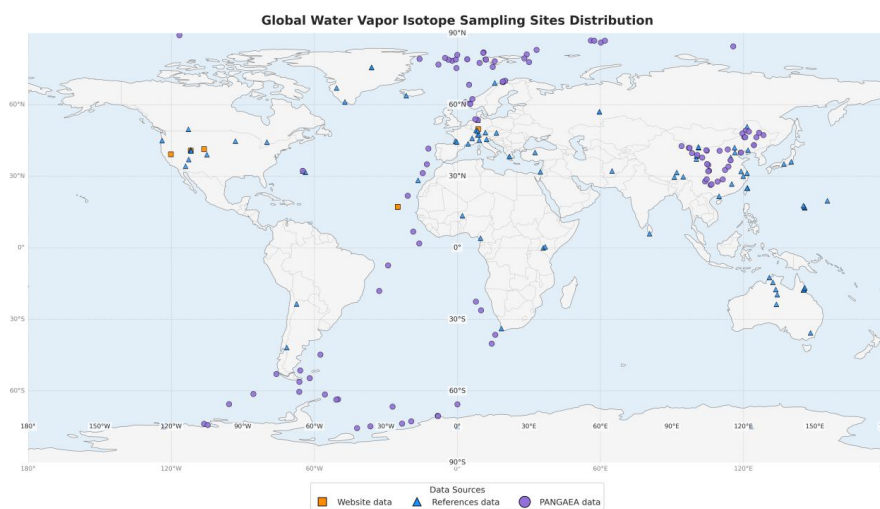
112 2.1 Data sources and collection

113 The dataset consists of three main components: data from the Global Network of
114 Isotopes in Water (<http://wateriso.utah.edu/waterisotopes>), data from the World Data
115 Center PANGAEA (<https://www.pangaea.de>), and isotopic data retrieved from
116 published literature. The dataset includes 87,138 records from various continents.
117 Literature-based data were systematically retrieved from the Web of Science database
118 using keyword combinations such as “isotope” and “atmospheric water,” along
119 with Boolean logic (Wang et al., 2023b). Based on quality control, targeted selection
120 and supplementation were carried out for underrepresented regions, thereby filling
121 spatial gaps and enhancing the dataset ’ s global representativeness and regional
122 coverage. We selected academic papers providing isotopic data in text, table, or figure
123 formats as the main data sources to improve data accuracy. The selected studies
124 explicitly identified the water type as "atmospheric water." In addition to isotopic data,
125 we also collected spatiotemporal information of sampling sites, including geographic
126 coordinates (latitude and longitude), exact sampling time, and elevation.

127 Moreover, the global climate classification data used in this study were derived
128 from the Köppen Global Climate Classification (Beck et al., 2018).

129

130



131

132 **Figure 1:** Spatial distribution of sampling sites in the global atmospheric water vapor stable
133 isotope dataset.

134 2.2 Instrumentation and measurement uncertainties

135 Atmospheric water vapor isotope observations included in this compilation
136 originate from heterogeneous measurement approaches. Because the dataset
137 aggregates values reported by different research groups rather than reprocessing raw
138 spectroscopic or mass-spectrometric signals, we document the instrumentation and
139 measurement method as reported in the original sources and summarize
140 major uncertainty drivers that users should consider when comparing records across
141 sites and platforms (Table S1).

142 2.2.1 In situ laser spectroscopy (Picarro CRDS and LGR OA-ICOS)

143 A substantial fraction of near-surface, high-frequency observations are based on
144 laser absorption spectroscopy, mainly cavity ring-down spectroscopy (CRDS)
145 analyzers from Picarro (e.g., L1102-i, L1115-i, L2120-i, L2130-i, L2140-i; model



146 names as reported) and off-axis integrated cavity output spectroscopy (OA-ICOS)
147 analyzers from Los Gatos Research (LGR) (e.g., WVIA series and related LGR
148 instruments; model names as reported). These instruments measure water vapor
149 mixing ratio and isotopic composition continuously, but their effective precision and
150 accuracy depend on humidity level, inlet configuration, calibration strategy, and
151 maintenance.

152 Key uncertainty sources for laser-based vapor isotope measurements include:

153 (i) humidity dependence of isotopic retrievals (especially at low water vapor
154 concentrations),

155 (ii) instrument drift and calibration-scale transfer to VSMOW,

156 (iii) memory effects caused by adsorption/desorption in tubing and internal
157 surfaces,

158 (iv) spectral interferences and pressure/temperature sensitivity, and

159 (v) condensation risks in sampling lines (which can induce fractionation).

160 Many source studies mitigate these effects using multi-point or two-point
161 calibration with laboratory standards and frequent checks; when such information is
162 explicitly reported, it is captured in the metadata fields of this dataset.

163 **2.2.2 Cryogenic trapping followed by IRMS**

164 Some records are derived from cryogenic trapping of atmospheric water vapor
165 (e.g., trapping at very low temperatures) followed by laboratory isotope-ratio mass
166 spectrometry (IRMS) of the condensed water (e.g., Finnigan/Thermo IRMS systems
167 such as DELTA V Plus with GasBench; other models as reported). IRMS typically



168 provides high analytical precision for $\delta^{18}\text{O}$ and $\delta^2\text{H}$ under controlled laboratory
169 conditions, but the overall uncertainty also reflects the vapor collection procedure.

170 Major additional uncertainty sources include:

- 171 (i) collection efficiency and representativeness of time-integrated samples,
- 172 (ii) potential fractionation during sampling/storage if evaporation occurs, and
- 173 (iii) blank effects or contamination in field handling.

174 Accordingly, IRMS-based values may be analytically precise yet temporally
175 averaged and method-dependent.

176 **2.2.3 Satellite retrieval products**

177 A limited subset of isotope information may come from satellite retrieval
178 products (e.g., TES on Aura retrieving δD_v from nadir-viewing infrared Fourier
179 transform spectroscopy). Satellite products represent retrieval-based estimates with
180 vertical sensitivity characteristics and averaging kernels; near-surface layers (e.g.,
181 900 hPa products used in some studies) should therefore be interpreted as retrieval
182 estimates rather than direct in situ measurements. Users should consider reported
183 retrieval precision, degrees of freedom of signal, and recommended quality flags in
184 the original product documentation.

185 **2.2.4 Practical implications for cross-study comparability**

186 To support reuse, we (i) record method class (in situ laser, cryogenic+IRMS,
187 satellite retrieval) and (ii) capture instrument/method/model information when
188 explicitly provided. Users conducting quantitative syntheses should account for
189 method-specific uncertainties and sampling representativeness, and are encouraged to



190 apply additional filters (e.g., humidity thresholds for laser instruments or product
191 quality flags for satellite retrievals) consistent with their scientific objectives.

192 **2.3 Data processing and quality control**

193 To ensure consistency across heterogeneous sources, we applied a standardized
194 harmonization and quality-control workflow to all records. This workflow focuses
195 on metadata and value integrity and preserves traceability to the original source.

196 (1) Data ingestion and formatting. Records were collected from wiDB,
197 PANGAEA, and peer-reviewed literature (tables, supplementary files). All fields
198 were converted into a unified tabular format with consistent variable names and units.

199 (2) Coordinate and time standardization. Site coordinates were harmonized to
200 WGS84 (latitude/longitude). Sampling time information was standardized to UTC
201 when sufficient information was available; otherwise, the reported local time and its
202 context were retained and flagged in metadata.

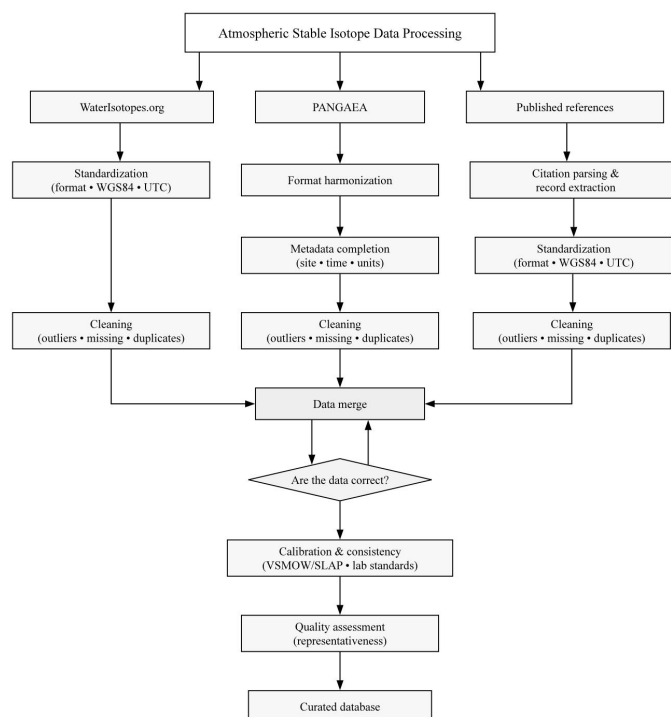
203 (3) Isotope notation and derived variables. Isotopic composition was stored in
204 delta notation in per mil (‰) relative to VSMOW as reported by the source. When
205 both $\delta^2\text{H}$ and $\delta^{18}\text{O}$ were available, d-excess was computed as $d = \delta^2\text{H} - 8 \delta^{18}\text{O}$. We
206 did not interpolate missing isotope values; missing entries remain as missing in the
207 dataset.

208 (4) Duplicate detection and traceability. Potential duplicates across sources (e.g.,
209 identical site/time/value combinations appearing in multiple repositories or
210 publications) were identified and consolidated while keeping the original source
211 references.

212 (5) Plausibility checks and QC flags. We screened for inconsistent metadata (e.g.,
213 impossible coordinates, swapped latitude/longitude, unrealistic elevations), unit
214 inconsistencies, and implausible isotope values. Records failing mandatory metadata
215 requirements or showing clear formatting errors were corrected when the original
216 source allowed unambiguous correction; otherwise, they were flagged. The dataset
217 includes QC indicators to allow users to filter data according to their tolerance for
218 uncertainty.



219



220

221 **Figure 2:** Data processing workflow of the global atmospheric water vapor stable isotope dataset.

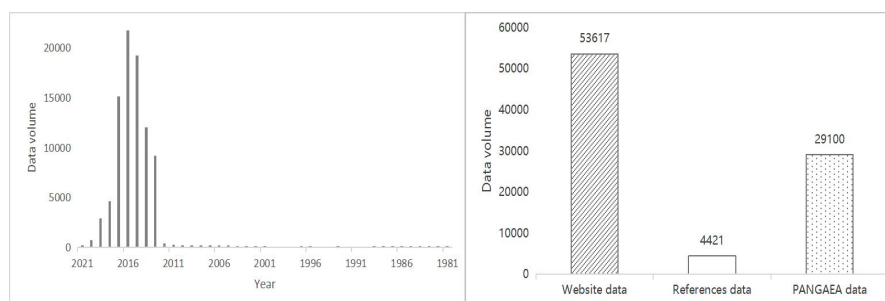
222 3 Dataset Description

223 3.1 Dataset Overview

224 This dataset comprises 87,138 measurements of hydrogen and oxygen stable
225 isotopes in atmospheric water vapor from 112 observation sites (Fig. 3). Specifically,
226 it includes 53,617 isotope records from 6 observation sites on the Global Water
227 Isotope Website, 29,100 records from 21 sites in the PANGAEA database, and 4,421
228 literature-derived records from 85 observation sites. We standardized and compiled
229 the scattered observational data into a unified dataset, achieving spatial coverage from
230 low to high latitudes and from continents to oceans. Importantly, the dataset covers



231 regions traditionally lacking observations, including Greenland, Iceland, Africa,
232 Antarctica, and adjacent oceanic areas, while maintaining dense observation sites in
233 key regions such as North America, the Mediterranean coast, and the western Pacific
234 margin, thus significantly enhancing global representativeness. The literature-derived
235 data span a wide temporal range, encompassing both high-frequency short-term
236 sequences and multi-year station or experimental observations. The PANGAEA data
237 are mainly distributed in the Atlantic Ocean and adjacent coastal regions, with
238 sampling largely derived from cruises or continuous station observations; these data
239 are temporally concentrated and highly continuous. Data from the Global Water
240 Isotope Website are more geographically clustered, primarily in mid-latitude inland
241 urban regions, with high sampling frequency and relatively continuous temporal
242 coverage.



243
244 **Figure 3:** Time series and categories of the global atmospheric water vapor stable isotope dataset.

245 **3.2 Spatiotemporal Patterns in Atmospheric Water Vapor Isotopes**

246 Based on water vapor isotope data collected from global observation stations and
247 reanalysis datasets, we standardized the data format and applied quality control,
248 calculated the deuterium excess (d-excess), and aggregated annual data by taking the
249 median within 3° grid cells. Spatial mapping employed segmented discrete color



250 scales to enhance regional comparability and suppress the influence of outliers. Figure
251 4 presents the global distributions of $\delta^2\text{H}$, $\delta^{18}\text{O}$, and d-excess under annual
252 conditions, while Figure 5 shows boxplot statistics for tropical, arid, temperate,
253 continental, and polar regions across the four seasons.

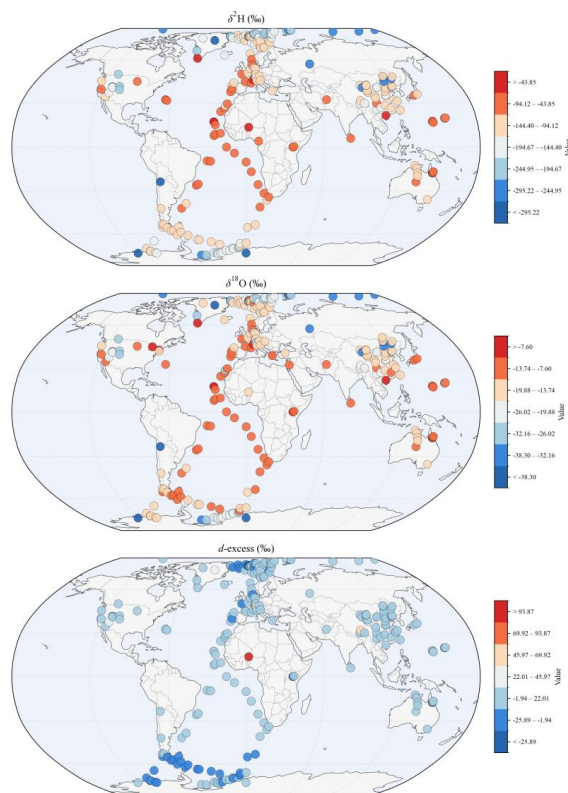
254 Spatially, both $\delta^2\text{H}$ and $\delta^{18}\text{O}$ exhibit a “double gradient”: enrichment at low
255 latitudes and depletion toward high latitudes; enrichment near the coastlines and
256 gradual depletion inland (Fig. 4). High values over subtropical to tropical oceans
257 indicate enrichment in warm, high-evaporation source regions; along the main
258 transport pathways extending inland and poleward, isotope ratios become
259 progressively lighter with decreasing temperature and stronger condensation (Ruan et
260 al., 2023), reaching the lowest values in polar regions. Pronounced gradients appear in
261 the transition zones between monsoon and westerly circulation systems and at
262 continental – oceanic boundaries. The d-excess demonstrates a complementary pattern:
263 it is higher over arid continents and subsidence zones, indicating enhanced
264 non-equilibrium evaporation and re-evaporation; it is lower over humid oceans and
265 deep convective regions, reflecting dominant near-equilibrium evaporation and strong
266 condensation processes.

267 Seasonally, all climate zones exhibit clear annual cyclic patterns, though
268 differing in amplitude and phase. The tropics show the smallest seasonal differences,
269 with slight enrichment in summer and depletion in winter. Arid regions exhibit the
270 largest amplitudes, with marked enrichment during summer due to non-equilibrium
271 evaporation, and depletion in autumn and winter as temperature and evaporation



272 decrease. Temperate regions display a “summer-enriched, winter-depleted” pattern,
273 consistent with their regional annual temperature variations. In continental regions,
274 long-range transport and re-evaporation amplify the seasonal amplitude, with the
275 lowest values in winter and secondary maxima in summer; spring shows increased
276 dispersion due to snowmelt and circulation transitions (Hua et al., 2017). Overall,
277 polar regions are the most depleted, with small amplitude — slight enrichment in
278 summer and the lowest values in winter under strong low-temperature fractionation.

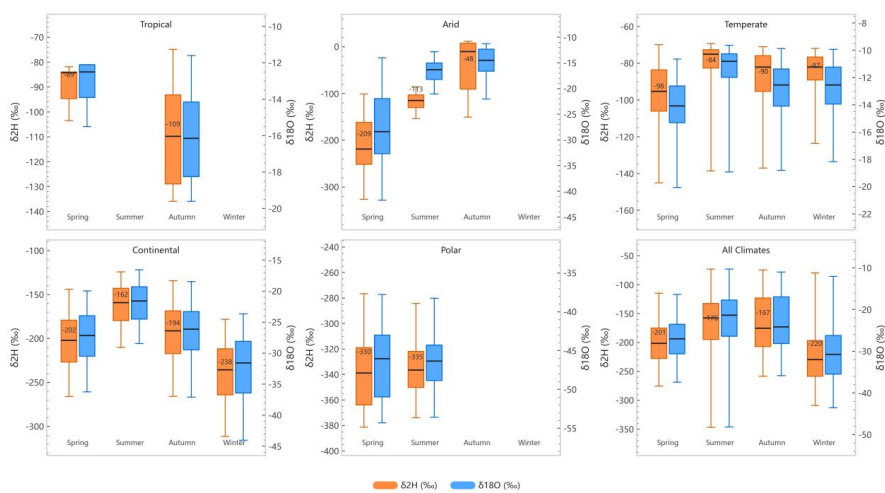
279 In terms of dispersion, arid and continental regions display the widest boxplots,
280 indicating a higher likelihood of extreme values under interannual climate variability
281 and surface heterogeneity (e.g., lake/river evaporation, irrigation recharge,
282 anthropogenic water use). The tropics and polar regions show smaller dispersions,
283 corresponding respectively to near-equilibrium processes under high humidity and
284 stable fractionation dominated by low temperatures. $\delta^2\text{H}$ and $\delta^{18}\text{O}$ display high
285 consistency in seasonal phase and stable amplitude ratios, indicating co-control by
286 evaporation – condensation processes. However, in arid regions and during summer,
287 $\delta^2\text{H}$ is more sensitive to non-equilibrium evaporation, showing stronger responses
288 than $\delta^{18}\text{O}$.



289

290

Figure 4: Spatial distribution of $\delta^2\text{H}$ and $\delta^{18}\text{O}$ in global atmospheric water vapor.



291

292

Figure 5: Seasonal variations of $\delta^2\text{H}$ and $\delta^{18}\text{O}$ in atmospheric water vapor across different climate

293

zones.



294 In summary, global atmospheric water vapor isotopes exhibit a spatial pattern of
295 “enrichment in low-latitude and arid regions, and depletion in high-latitude and inland
296 areas.” Temporally, isotope variations are coupled with temperature and evaporation:
297 amplitudes are larger in arid and continental regions, but smaller in tropical and polar
298 regions.

299 3.3 Uncertainty and outlook

300 At present, limited by sampling technologies and methods, the sampling
301 frequency, observation duration, and analytical procedures vary across different
302 climatic regimes. The spatial distribution of observation sites is uneven, and the
303 establishment of long-term continuous monitoring is constrained by cost, labor,
304 equipment, and environmental conditions. Consequently, data continuity and
305 completeness across spatial and temporal scales remain limited—especially in
306 high-latitude regions and harsh environments such as deserts and rainforests, where
307 observations are sparse—thus constraining the reliability of regional comparisons
308 (Smedsrud et al., 2022). In addition, differences in sample preservation conditions,
309 analytical techniques, and instrument precision may introduce systematic errors,
310 reducing the comparability and overall reliability of multi-source datasets. Although
311 the present study applies unified calibration as far as possible, achieving consistency
312 and precision at a global scale remains a significant challenge.

313 In the future, continuous high-frequency observation networks could be
314 established in data-sparse regions such as arid zones and polar areas to reduce
315 uncertainties in quantifying nonequilibrium processes and moisture recycling (Zhu et



316 al., 2022). Unified standards for sampling, preservation, analysis, and quality control
317 should be established and promoted. In addition, metadata cataloging and traceable
318 data sharing should be improved to build a high-quality global atmospheric water
319 isotope database. On this basis, multi-source integration of ground-based,
320 remote-sensing, and reanalysis datasets should be advanced (Li et al., 2024). By
321 coupling artificial intelligence with reanalysis products (e.g., ERA5, MERRA-2) and
322 applying multivariate decomposition and causal inference frameworks, contributions
323 of driving factors can be quantitatively assessed. Consequently, this would enable
324 robust characterization of evaporation–transport–condensation linkages and recycling
325 processes, narrowing structural and parametric uncertainties, improving predictability
326 from event to decadal scales, and elevating isotopes from “tracer information” to
327 “decision variables.” Such progress would provide traceable evidence for drought
328 early warning, extreme precipitation attribution, ecological water allocation, and
329 cross-regional coordination—thus supporting higher-quality water and climate
330 governance with reduced uncertainty (Grafton et al., 2013).

331 **4 Data availability**

332 The global atmospheric water vapor stable isotope dataset has been publicly
333 released and is available at <https://doi.org/10.6084/m9.figshare.30893984> (Zhu and
334 Yang, 2025). Files and accompanying metadata (e.g., variable definitions, source
335 references, and processing notes) are provided on the repository landing page. Users
336 are encouraged to cite the DOI and the original data sources when reusing the dataset.

337 **5 Conclusion**



338 This data description paper delivers a traceable, harmonized compilation of
339 near-surface atmospheric water vapor stable isotopes (reported as $\delta^2\text{H}$ and $\delta^{18}\text{O}$
340 relative to VSMOW) by integrating three complementary sources: the WaterIsotopes
341 Database (wiDB), PANGAEA, and peer-reviewed literature. The primary
342 contribution is not a new interpretation of vapor isotope variability, but a documented
343 workflow that converts heterogeneous observations into a single product that is easier
344 to discover, filter, and reuse across disciplines and regions.

345 To construct the dataset, we consolidated records from repositories and
346 publications into a unified tabular structure and preserved links to original sources for
347 each entry. We standardized spatial metadata by harmonizing coordinates to WGS84
348 and checked for common geolocation issues. We harmonized temporal information by
349 converting timestamps to UTC when sufficient time-zone information was available,
350 while retaining and flagging records whose time reference could not be
351 unambiguously converted. Isotope values were stored consistently in delta notation in
352 per mil (‰) on the VSMOW scale as reported by the source, and d-excess was
353 computed where both $\delta^2\text{H}$ and $\delta^{18}\text{O}$ were available. Importantly, We did not attempt
354 to enforce data continuity by filling gaps (e.g., via interpolation or other imputation
355 methods); instead, we retained missing entries as missing to preserve the original
356 values and their reported accuracy.

357 Because comparability depends strongly on measurement strategy, we compiled
358 instrumentation metadata (instrument/method/model when explicitly reported) and
359 categorized observations by method class, including in situ laser spectroscopy



360 (Picarro CRDS; LGR OA-ICOS), cryogenic trapping followed by IRMS, and satellite
361 retrieval products. We applied transparent quality-control checks to identify duplicates
362 across sources, inconsistent metadata, unit/format issues, and implausible or poorly
363 documented records, using QC flags to support user-defined filtering while
364 maintaining traceability.

365 The resulting dataset is intended to support (i) evaluation and benchmarking of
366 isotope-enabled models, (ii) cross-site comparisons under different climates and
367 observation protocols, and (iii) synthesis studies of boundary-layer and
368 land-atmosphere water-cycle processes. Users are encouraged to account for
369 method-dependent uncertainties and sampling representativeness using the provided
370 metadata and QC indicators. Future updates can extend temporal coverage,
371 incorporate newly published datasets, and improve the completeness of instrument
372 and calibration documentation where available.

373

374 **Author contributions**

375 Dongfei Yang: Writing-Original draft preparation; Guofeng Zhu:
376 Writing-Reviewing and Editing; Jiangwei Yang: Methodology; Rui Li: Methodology;
377 Qinqin Wang: Validation; Xiaoxiao Su: Investigation; Yitian Lei: Investigation;
378 Yurou Zhang: Investigation; Wenjing Liu: Investigation; Kang Ning: Investigation;
379 Xinyue Wang: Investigation; Yaxin Li: Investigation;

380 **Conflict of Interest Statement**

381 The authors declare that they have no known competing financial interests or



382 personal relationships that could have appeared to influence the work reported in this
383 paper.

384 **Disclaimer**

385 Publisher's note: Copernicus Publications remains neutral with regard to
386 jurisdictional claims made in the text, published maps, institutional affiliations, or any
387 other geographical representation in this paper. While Copernicus Publications makes
388 every effort to include appropriate place names, the final responsibility lies with the
389 authors.

390 **Acknowledgments**

391 The authors would like to thank Gabriel J. Bowen for his contributions to the
392 wiDB database and the International colleagues for their outstanding contributions
393 with respect to the World Data Center PANGAEA dataset. Finally, the authors thank
394 all of the researchers and institutions that provided data.

395 **Financial support**

396 This research was financially supported by the National Natural Science
397 Foundation of China (42371040), the Key Natural Science Foundation of Gansu
398 Province (23JRRA698), the Western Light Young Scholars Program of the Chinese
399 Academy of Sciences(25JR6KA001),the Key Research and Development Program of
400 Gansu Province (22YF7NA122), the Gansu Provincial Basic Research Innovation
401 Group Project (22JR5RA129), the Water Resources Science Experimental Research
402 and Technology Promotion Project of Gansu Provincial(25GSLK062), the Cultivation
403 Program of Major key projects of Northwest Normal University



404 (NWNLU-LKZD-202302), the Oasis Scientific Research achievements Breakthrough
405 Action Plan Project of Northwest normal University (NWNLU-LZKX-202303), the
406 Special Project on Rural Revitalization and Food Security of the Ministry of
407 Agriculture and Rural Affairs.



408 References

- 409 Baijuan, Z., Zongxing, L., Qi, F., Baiting, Z., and Juan, G.: A review of isotope
410 ecohydrology in the cold regions of Western China, *Sci. Total Environ.*, 857,
411 159438, <https://doi.org/10.1016/j.scitotenv.2022.159438>, 2023.
- 412 Beck, H. E., Zimmermann, N. E., McVicar, T. R., Vergopolan, N., Berg, A., and Wood,
413 E. F.: Present and future Köppen-Geiger climate classification maps at 1-km
414 resolution, *Sci. Data*, 5, 180214, <https://doi.org/10.1038/sdata.2018.214>, 2018.
- 415 Bingham, F. M. and Bayler, E.: Intensifying Seasonality of the Global Water Cycle as
416 Indicated by Sea Surface Salinity, *Geophys. Res. Lett.*, 52, e2024GL111608,
417 <https://doi.org/10.1029/2024GL111608>, 2025.
- 418 Chen, L., Wang, Q., Zhu, G., Lin, X., Qiu, D., Jiao, Y., Lu, S., Li, R., Meng, G., and
419 Wang, Y.: Dataset of stable isotopes of precipitation in the Eurasian continent,
420 *Earth Syst. Sci. Data*, 16, 1543–1557, <https://doi.org/10.5194/essd-16-1543-2024>,
421 2024.
- 422 Colman, R. and Soden, B. J.: Water vapor and lapse rate feedbacks in the climate
423 system, *Rev. Mod. Phys.*, 93, 045002,
424 <https://doi.org/10.1103/RevModPhys.93.045002>, 2021.
- 425 Fang, L., Gao, R., Wang, X., and Liu, T.: Isotopes-based characterization of
426 precipitation compositions and atmospheric water vapor sources over typical
427 Eurasian steppes in south mongolian Plateau, *J. Hydrol.*, 615, 128724,
428 <https://doi.org/10.1016/j.jhydrol.2022.128724>, 2022.
- 429 Galewsky, J., Steen-Larsen, H. C., Field, R. D., Worden, J., Risi, C., and Schneider,
430 M.: Stable isotopes in atmospheric water vapor and applications to the
431 hydrologic cycle, *Rev. Geophys.*, 54, 809–865,
432 <https://doi.org/10.1002/2015RG000512>, 2016.
- 433 Galewsky, J., Schneider, M., Diekmann, C., Semie, A., Bony, S., Risi, C., Emanuel,
434 K., and Brogniez, H.: The Influence of Convective Aggregation on the Stable
435 Isotopic Composition of Water Vapor, *AGU Adv.*, 4, e2023AV000877,
436 <https://doi.org/10.1029/2023AV000877>, 2023.
- 437 Gimeno, L., Vázquez, M., Eiras-Barca, J., Sorí, R., Stojanovic, M., Algarra, I., Nieto,
438 R., Ramos, A. M., Durán-Quesada, A. M., and Dominguez, F.: Recent progress
439 on the sources of continental precipitation as revealed by moisture transport
440 analysis, *Earth-Sci. Rev.*, 201, 103070,
441 <https://doi.org/10.1016/j.earscirev.2019.103070>, 2020.
- 442 Gimeno, L., Eiras-Barca, J., Durán-Quesada, A. M., Dominguez, F., Van Der Ent, R.,
443 Sodemann, H., Sánchez-Murillo, R., Nieto, R., and Kirchner, J. W.: The
444 residence time of water vapour in the atmosphere, *Nat. Rev. Earth Environ.*, 2,
445 558–569, <https://doi.org/10.1038/s43017-021-00181-9>, 2021.
- 446 Grafton, R. Q., Pittock, J., Davis, R., Williams, J., Fu, G., Warburton, M., Udall, B.,
447 McKenzie, R., Yu, X., Che, N., Connell, D., Jiang, Q., Kompas, T., Lynch, A.,
448 Norris, R., Possingham, H., and Quiggin, J.: Global insights into water resources,
449 climate change and governance, *Nat. Clim. Change*, 3, 315–321,
450 <https://doi.org/10.1038/nclimate1746>, 2013.



- 451 Hua, L., Zhong, L., and Ma, Z.: Decadal Transition of Moisture Sources and
452 Transport in Northwestern China During Summer From 1982 to 2010, *J.*
453 *Geophys. Res. Atmospheres*, 122, <https://doi.org/10.1002/2017JD027728>, 2017.
- 454 Jouzel, J., Delaygue, G., Landais, A., Masson-Delmotte, V., Risi, C., and Vimeux, F.:
455 Water isotopes as tools to document oceanic sources of precipitation, *Water*
456 *Resour. Res.*, 49, 7469–7486, <https://doi.org/10.1002/2013WR013508>, 2013.
- 457 Klein, E. S., Cherry, J. E., Young, J., Noone, D., Leffler, A. J., and Welker, J. M.:
458 Arctic cyclone water vapor isotopes support past sea ice retreat recorded in
459 Greenland ice, *Sci. Rep.*, 5, 10295, <https://doi.org/10.1038/srep10295>, 2015.
- 460 Leroy-Dos Santos, C., Fourré, E., Agosta, C., Casado, M., Cauquoin, A., Werner, M.,
461 Minster, B., Prié, F., Jossoud, O., Petit, L., and Landais, A.: From atmospheric
462 water isotopes measurement to firn core interpretation in Adélie Land: a case
463 study for isotope-enabled atmospheric models in Antarctica, *The Cryosphere*, 17,
464 5241–5254, <https://doi.org/10.5194/tc-17-5241-2023>, 2023.
- 465 Li, R., Zhu, G., Chen, L., Qi, X., Lu, S., Meng, G., Wang, Y., Li, W., Zheng, Z., Yang,
466 J., and Gun, Y.: Global Stable Isotope Dataset for Surface Water, *Earth Syst. Sci.*
467 *Data*, 17, 2135–2145, <https://doi.org/10.5194/essd-17-2135-2025>, 2025.
- 468 Li, S., Han, Y., Li, C., and Wang, J.: A novel framework for multi-layer soil moisture
469 estimation with high spatio-temporal resolution based on data fusion and
470 automated machine learning, *Agric. Water Manag.*, 306, 109173,
471 <https://doi.org/10.1016/j.agwat.2024.109173>, 2024.
- 472 Lu, S., Zhu, G., Meng, G., Lin, X., Liu, Y., Qiu, D., Xu, Y., Wang, Q., Chen, L., Li, R.,
473 and Jiao, Y.: Influence of atmospheric circulation on the stable isotope of
474 precipitation in the monsoon margin region, *Atmospheric Res.*, 298, 107131,
475 <https://doi.org/10.1016/j.atmosres.2023.107131>, 2024.
- 476 Peng, P., John Zhang, X., and Chen, J.: Bias correcting isotope-equipped GCMs
477 outputs to build precipitation oxygen isoscape for eastern China, *J. Hydrol.*, 589,
478 125153, <https://doi.org/10.1016/j.jhydrol.2020.125153>, 2020.
- 479 Ren, Y., Yu, H., Huang, J., Peng, M., and Zhou, J.: The Projected Response of the
480 Water Cycle to Global Warming Over Drylands in East Asia, *Earths Future*, 12,
481 e2023EF004008, <https://doi.org/10.1029/2023EF004008>, 2024.
- 482 Rozmiarek, K. S., Dietrich, L. J., Vaughn, B. H., Town, M. S., Markle, B. R., Morris,
483 V., Steen-Larsen, H. C., Fettweis, X., Brashear, C. A., Bennett, H., and Jones, T.
484 R.: Atmosphere to Surface Profiles of Water-Vapor Isotopes and Meteorological
485 Conditions Over the Northeast Greenland Ice Sheet, *J. Geophys. Res.*
486 *Atmospheres*, 130, e2024JD042719, <https://doi.org/10.1029/2024JD042719>,
487 2025.
- 488 Ruan, K., Lin, Y., Yang, P., and Zhou, W.: Condensation matters, *Nat. Chem. Biol.*, 19,
489 1180–1182, <https://doi.org/10.1038/s41589-023-01415-1>, 2023.
- 490 Saranya, P., Krishan, G., Rao, M. S., Kumar, S., and Kumar, B.: Controls on water
491 vapor isotopes over Roorkee, India: Impact of convective activities and
492 depression systems, *J. Hydrol.*, 557, 679–687,
493 <https://doi.org/10.1016/j.jhydrol.2017.12.061>, 2018.
- 494 Shang, B., Gao, J., Chen, G., and Wu, Y.: Stable isotopes in atmospheric water vapour:



- 495 Patterns, mechanisms and perspectives, *Sci. China Earth Sci.*, 67, 3789–3813,
496 <https://doi.org/10.1007/s11430-023-1410-6>, 2024.
- 497 Shi, M., Worden, J. R., Bailey, A., Noone, D., Risi, C., Fu, R., Worden, S., Herman, R.,
498 Payne, V., Pagano, T., Bowman, K., Bloom, A. A., Saatchi, S., Liu, J., and Fisher,
499 J. B.: Amazonian terrestrial water balance inferred from satellite-observed water
500 vapor isotopes, *Nat. Commun.*, 13, 2686,
501 <https://doi.org/10.1038/s41467-022-30317-4>, 2022.
- 502 Smedsrud, L. H., Muilwijk, M., Brakstad, A., Madonna, E., Lauvset, S. K.,
503 Spensberger, C., Born, A., Eldevik, T., Drange, H., Jeansson, E., Li, C., Olsen, A.,
504 Skagseth, Ø., Slater, D. A., Straneo, F., Våge, K., and Årthun, M.: Nordic Seas
505 Heat Loss, Atlantic Inflow, and Arctic Sea Ice Cover Over the Last Century, *Rev.*
506 *Geophys.*, 60, e2020RG000725, <https://doi.org/10.1029/2020RG000725>, 2022.
- 507 Smith, A. C. and Lacey, J. H.: Tracing anthropogenic climate and environmental
508 change using stable isotopes, *Quat. Sci. Rev.*, 346, 109028,
509 <https://doi.org/10.1016/j.quascirev.2024.109028>, 2024.
- 510 Tharammal, T., Bala, G., and Nusbaumer, J. M.: Sources of water vapor and their
511 effects on water isotopes in precipitation in the Indian monsoon region: a
512 model-based assessment, *Sci. Rep.*, 13, 708,
513 <https://doi.org/10.1038/s41598-023-27905-9>, 2023.
- 514 Voglar, G. E., Zavadlav, S., Levanič, T., and Ferlan, M.: Measuring techniques for
515 concentration and stable isotopologues of CO₂ in a terrestrial ecosystem: A
516 review, *Earth-Sci. Rev.*, 199, 102978,
517 <https://doi.org/10.1016/j.earscirev.2019.102978>, 2019.
- 518 Wang, D., Tian, L., Risi, C., Wang, X., Cui, J., Bowen, G. J., Yoshimura, K., Wei, Z.,
519 and Li, L. Z. X.: Vehicle-based in situ observations of the water vapor isotopic
520 composition across China: spatial and seasonal distributions and controls,
521 *Atmospheric Chem. Phys.*, 23, 3409–3433,
522 <https://doi.org/10.5194/acp-23-3409-2023>, 2023a.
- 523 Wang, Y., Sun, Q., Yu, J., Xu, N., Wei, Y., Cho, J. H., and Wang, Z. L.: Boolean Logic
524 Computing Based on Neuromorphic Transistor, *Adv. Funct. Mater.*, 33, 2305791,
525 <https://doi.org/10.1002/adfm.202305791>, 2023b.
- 526 Wei, Z., Lee, X., Aemisegger, F., Benetti, M., Berkelhammer, M., Casado, M., Caylor,
527 K., Christner, E., Dyroff, C., García, O., González, Y., Griffis, T., Kurita, N.,
528 Liang, J., Liang, M.-C., Lin, G., Noone, D., Gribanov, K., Munksgaard, N. C.,
529 Schneider, M., Ritter, F., Steen-Larsen, H. C., Vallet-Coulomb, C., Wen, X.,
530 Wright, J. S., Xiao, W., and Yoshimura, K.: A global database of water vapor
531 isotopes measured with high temporal resolution infrared laser spectroscopy, *Sci.*
532 *Data*, 6, 180302, <https://doi.org/10.1038/sdata.2018.302>, 2019.
- 533 Xing, M., Wang, Z., and Dong, J.: The premise of temperature effect playing in
534 regions with complex moisture sources – Evidence from high-resolution water
535 vapor isotopes, *J. Hydrol.*, 623, 129827,
536 <https://doi.org/10.1016/j.jhydrol.2023.129827>, 2023.
- 537 Xu, T., Pang, H., Zhan, Z., Zhang, W., Guo, H., Wu, S., and Hou, S.: Water vapor
538 isotopes indicating rapid shift among multiple moisture sources for the



- 539 2018–2019 winter extreme precipitation events in southeastern China, *Hydrol.*
540 *Earth Syst. Sci.*, 26, 117–127, <https://doi.org/10.5194/hess-26-117-2022>, 2022.
- 541 Xu, W., Xia, X., Piao, S., Wu, D., Li, W., Yang, S., and Yuan, W.: Weakened Increase
542 in Global Near-Surface Water Vapor Pressure During the Last 20 Years, *Geophys.*
543 *Res. Lett.*, 51, e2023GL107909, <https://doi.org/10.1029/2023GL107909>, 2024.
- 544 Yang, G., Xiao, Y., Wang, S., Qian, Y., Li, H., and Zhang, M.: Satellite-Based
545 Distribution of Inverse Altitude Effect of Global Water Vapor Isotopes: Potential
546 Influences on Isotopes in Climate Proxies, *Remote Sens.*, 15, 4533,
547 <https://doi.org/10.3390/rs15184533>, 2023.
- 548 Zhu, G. and Yang, dongfei: Global Water Vapor Stable Isotope Dataset,
549 <https://doi.org/10.6084/M9.FIGSHARE.30893984>, 2025.
- 550 Zhu, G., Liu, Y., Shi, P., Jia, W., Zhou, J., Liu, Y., Ma, X., Pan, H., Zhang, Y., Zhang,
551 Z., Sun, Z., Yong, L., and Zhao, K.: Stable water isotope monitoring network of
552 different water bodies in Shiyang River basin, a typical arid river in China, *Earth*
553 *Syst. Sci. Data*, 14, 3773–3789, <https://doi.org/10.5194/essd-14-3773-2022>,
554 2022.
- 555 Zhu, G., Liu, Y., Wang, L., Sang, L., Zhao, K., Zhang, Z., Lin, X., and Qiu, D.: The
556 isotopes of precipitation have climate change signal in arid Central Asia, *Glob.*
557 *Planet. Change*, 225, 104103, <https://doi.org/10.1016/j.gloplacha.2023.104103>,
558 2023.
- 559